JACS
JOURNAL OF THE AMERICAN CHEMICAL SOCIETY
Article
pubs.acs.org/JACS

Extrinsic Hardening of Superhard Tungsten Tetraboride Alloys with Group 4 Transition Metals

Georgiy Akopov,[†] Michael T. Yeung,[†] Christopher L. Turner,[†] Reza Mohammadi,[‡] and Richard B. Kaner*[,†,§,∥]

[†]Department of Chemistry and Biochemistry, [§]Department of Materials Science and Engineering, and [∥]California NanoSystems Institute (CNSI), University of California, Los Angeles (UCLA), Los Angeles, California 90095, United States

[‡]Department of Mechanical and Nuclear Engineering, Virginia Commonwealth University, Richmond, Virginia 23284, United States

Supporting Information

ABSTRACT: Alloys of tungsten tetraboride (WB_4) with the group 4 transition metals, titanium (Ti), zirconium (Zr), and hafnium (Hf), of different concentrations (0−50 at. % on a metals basis) were synthesized by arc-melting in order to study their mechanical properties. The phase composition and purity of the as-synthesized samples were confirmed using powder X-ray diffraction (PXRD) and energy dispersive X-ray spectroscopy (EDS). The solubility limit as determined by PXRD is 20 at. % for Ti, 10 at. % for Zr, and 8 at. % for Hf. Vickers indentation measurements of WB_4 alloys with 8 at. % Ti, 8 at. % Zr, and 6 at. % Hf gave hardness values, H_v, of 50.9 ± 2.2, 55.9 ± 2.7 and 51.6 ± 2.8 GPa, respectively, compared to 43.3 GPa for pure WB_4 under an applied load of 0.49 N. Each of the aforementioned compositions are considered superhard (H_v > 40 GPa), likely due to extrinsic hardening that plays a key role in these superhard metal borides. Furthermore, these materials exhibit a significantly reduced indentation size effect, which can be seen in the plateauing hardness values for the $W_{1-x}Zr_xB_4$ alloy. In addition, $W_{0.92}Zr_{0.08}B_4$, a product of spinoidal decomposition, possesses nanostructured grains and enhanced grain hardening. The hardness of $W_{0.92}Zr_{0.08}B_4$ is 34.7 ± 0.65 GPa under an applied load of 4.9 N, the highest value obtained for any superhard metal at this relatively high loading. In addition, the WB_4 alloys with Ti, Zr, and Hf showed a substantially increased oxidation resistance up to ∼460 °C, ∼510 °C, and ∼490 °C, respectively, compared to ∼400 °C for pure WB_4.

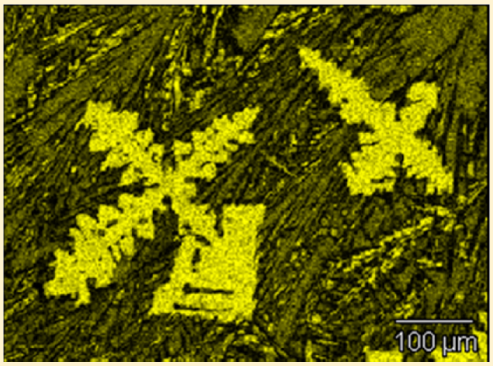

INTRODUCTION

Diamond is the hardest mineral because of its structure. The high density of carbon atoms produces ultra-incompressibility, while the large number of short covalent bonds gives rise to its extreme shear modulus. Together, these attributes make natural diamond superhard; as such, diamond is commonly used in the oil industry for cutting and drilling. Unfortunately, both natural diamond, due to its limited supply, and synthetic diamond, due to the high pressure and high temperature needed for its synthesis, are expensive. Diamond cutting tools cannot be used to cut ferrous metals such as steel due to the formation of brittle carbides. Therefore, most cutting tools are made out of less expensive materials such as tungsten carbide (WC). Since WC is a hard metal, it can be readily cut and shaped using electric discharge machining. However, WC is not that hard (H_v = 25 GPa),[1] so the development of superhard metals (H_v > 40 GPa) is becoming an increasingly important area for exploration.

The primary focus for the development of superhard metals to date has been on new compositions and crystal structures. Metal borides represent an interesting class of covalent, yet metallic compounds, with a wide range of mechanical, thermal, and electronic properties.[2−5] These compounds exhibit a variety of crystal lattices with different arrangements of boron atoms, ranging from isolated borons ($Cr_2B_{(rhomb)}$) to boron networks ($TaB_{2(hex)}$) to a boron skeleton ($UB_{12(cub)}$, $YB_{66(cub)}$).[2,3] While intrinsically related structural and mechanical properties[1] are fundamental to the development of such materials, there is a strong possibility that overall hardness can be dramatically enhanced following a completely orthogonal approach, i.e., through extrinsic effects. More intriguingly, all of these new borides are metallic; meaning that unlike natural diamond, conventional metallurgical techniques such as dispersion, precipitation, or grain boundary hardening can be used to strengthen them.

Among the different borides, tungsten tetraboride (WB_4, $P6_3/mmc$, Inorganic Crystal Structure Database, ICSD, 291124) represents a very interesting system due to its unique defect structure, which allows for hosting a wide variety of other transition metals in its lattice to form alloys (Figure 1).[6−9] Previous work has shown that adding different transition metals can dramatically increase the hardness and mechanical properties of WB_4 alloys, which intrinsically is already superhard (Vickers hardness $H_v \geq 40$ GPa).[7,8,10]

Received: March 12, 2016
Published: April 26, 2016

DOI: 10.1021/jacs.6b02676
J. Am. Chem. Soc. 2016, 138, 5714−5721

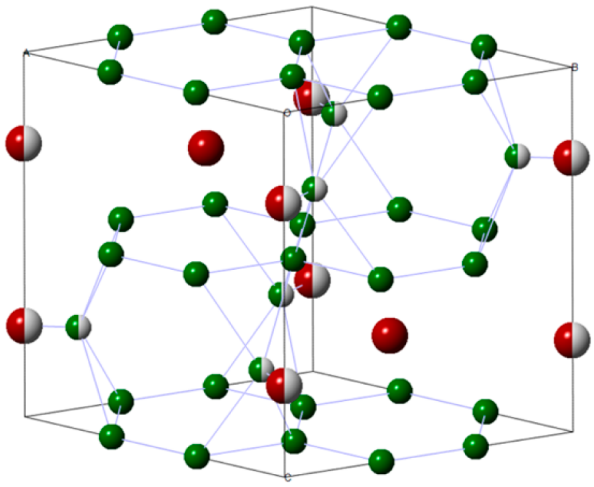

Figure 1. Crystal structure of tungsten tetraboride (WB_4, $P6_3/mmc$, Inorganic Crystal Structure Database, ICSD, 291124). Boron atoms are represented in green, and tungsten atoms are shown in maroon; the half-filled atoms show partially occupied positions.

Here, we report on WB_4 alloys with Ti, Zr, and Hf, and how changes and differences in structure and grain morphology affect the hardness and thermal stability. Likely mechanisms behind the changes in properties are provided in each case. In this way, we demonstrate that unlike diamond, superhard metal borides are metals, for which conventional hardening mechanisms are applicable even in the superhard regime.

EXPERIMENTAL PROCEDURE

In order to prepare samples of WB_4 and its alloys with Ti, Zr, and Hf, powders of high-purity were used: tungsten (99.95%, Strem Chemicals, U.S.A.), amorphous boron (99+%, Strem Chemicals, U.S.A.), titanium (99%, Johnson Matthey Chemical Products, U.S.A.), zirconium (99.5%, Strem Chemicals, U.S.A.), and hafnium (99.8%, Materion, U.S.A.). The molar ratios of tungsten to boron were kept at 1:12 in order to prevent the formation of secondary boride phases of tungsten (e.g., WB_2).[8,11] The powders of the appropriate metals were weighed according to the calculated values for each sample of the alloys of WB_4 with Ti, Zr and Hf: $W_{1-x}Ti_xB_4$, $W_{1-x}Zr_xB_4$ and $W_{1-x}Hf_xB_4$ (x = 0.0−0.5). To ensure that each mixture was homogeneous, the powders were then thoroughly mixed in an agate mortar using a pestle. The sample mixtures were then pressed into pellets using a hydraulic press (Carver) with an applied load of 10 tons. The pressed samples were then placed into an arc-melter chamber on top of a water-cooled copper hearth and arc-melted in an argon atmosphere using a current of 70 A for 1−2 min.

In order to carry out further analysis, each arc-melted sample was cut into two halves using a diamond saw (Ameritool Inc., U.S.A.). The first half was crushed using a tool steel Plattner-style diamond crusher into a fine sub-40 μm powder and used for powder X-ray diffraction (PXRD) analysis. The second half was prepared for hardness measurements and energy-dispersive X-ray spectroscopy (EDS) analysis by encapsulation in epoxy using an epoxy/hardener set (Allied High Tech Products Inc., U.S.A.). The samples were polished to an optically flat surface using a polishing station (South Bay Technology Inc., U.S.A.) and silicon carbide papers of 120−1200 grit sizes (Allied High Tech Products Inc., U.S.A.), followed by diamond films with particle sizes ranging from 30 to 1 μm (South Bay Technology Inc., U.S.A.).

The samples were then subjected to PXRD analysis and EDS analysis in order to verify the composition and purity of the boride phases. PXRD analysis was carried out on the crushed powder samples using a Bruker D8 Discover Powder X-ray Diffractometer (Bruker Corporation, Germany). PXRD patterns were collected using a $Cu_{K\alpha}$ X-ray beam (λ = 1.5418 Å) in the 5−100° 2θ range with a step size of 0.0353°, scan speed of 0.1055°/s, and time per step of 0.3 s. The collected patterns were then cross-referenced against the patterns in the database of the Joint Committee on Powder Diffraction Standards (JCPDS) to identify the phases present in the XRD patterns. The polished samples were checked for phase purity using an UltraDry EDS detector (Thermo Scientific, U.S.A.) attached to an FEI Nova 230 high-resolution scanning electron microscope (FEI Company, U.S.A.).

Hardness measurements were performed on the polished samples using a MicroMet 2103 Vickers microhardness tester (Buehler Ltd., U.S.A.) with a pyramidal diamond indenter tip. Each sample was indented 20 times at randomly chosen spots with an applied load of 0.49, 0.98, 1.96, 2.94, and 4.9 N of force. In order to calculate the Vickers hardness values (H_v, in GPa), the diagonals of each indent were measured under a total magnification of 500× using a high-resolution optical microscope, Zeiss Axiotech 100HD (Carl Zeiss Vision GmbH, Germany) and the following formula was used (eq 1):

$$H_v = \frac{1854.4F}{d^2} \quad (1)$$

where F is the applied load in Newtons (N) and d is the arithmetic average length of the diagonals of each indent in microns. The hardness values for all 20 indents for each respective loading were then averaged and plotted on hardness graphs (Figure 3a−c). All calculated average hardness values under each applied load of 0.49, 0.98, 1.96, 2.94, and 4.9 N have a standard deviation within 4.31, 3.45, 2.92, 2.03, and 1.41 GPa, respectively.

Thermogravimetric analysis (TGA) was performed using a Pyris Diamond TGA/DTA unit (TG-DTA, PerkinElmer Instruments, U.S.A.). The samples were heated in air from 25 to 200 °C at a rate of 20 °C/min, held at 200 °C for 30 min to remove any moisture, heated from 200 to 1000 °C at a rate of 2 °C/min, held at 1000 °C for 2 hr and then cooled from 1000 to 25 °C at a rate of 5 °C/min. In order to identify the resulting phase(s), XRD analysis was performed.

RESULTS AND DISCUSSION

The work here investigates the effects of group 4 transition metals (titanium, zirconium, and hafnium) on the hardness and thermal stability of the resulting alloys formed with tungsten tetraboride: $W_{1-x}Ti_xB_4$, $W_{1-x}Zr_xB_4$, and $W_{1-x}Hf_xB_4$, where x = 0.0−0.5. The relatively small atomic size of tungsten (W = 1.35 Å)[12] means that titanium (Ti = 1.40 Å)[12] is slightly larger than tungsten, while zirconium (Zr = 1.55 Å)[12] and hafnium (Hf = 1.55 Å)[12] are considerably larger. According to the Hume−Rothery rules, in order to form a thermodynamically favorable solid solution, the solute's: (1) radius must differ by <15%; (2) crystal structure must be similar; (3) oxidation states must be similar; and (4) electronegativity must be similar to that of the host material.[13] Therefore, it is not surprising that group 4 transition metals do indeed form limited solid solutions with WB_4 (i.e., <20 at. % for Ti, 10 at. % for Zr and below 8 at. % for Hf as will be seen) and form secondary phases at higher concentrations of solute (Scheme 1). Moreover, the highest boride (the most boron-rich compound in the phase diagram) of titanium (TiB_2), zirconium (ZrB_{12}), and hafnium (HfB_2) vary, which is especially prominent in the case of the latter two metals. The atomic radii of Zr and Hf differ in a 12-coordinate environment, with Hf being slightly smaller than Zr, resulting in only zirconium possessing a dodecaboride phase (ZrB_{12}).[14,15] On the other hand, hafnium readily forms a "β-rhombohedral boron doping phase" −HfB_{50} (Figure S1). This phase of boron represents a solid solution of hafnium in β-rhombohedral boron. The main difference between this phase and pure β-rhombohedral boron is the substitution of some of the boron icosahedra for Hf atoms. Note that the β-rhombohedral boron

DOI: 10.1021/jacs.6b02676
J. Am. Chem. Soc. 2016, 138, 5714−5721

Scheme 1. Phase Formation Based on the Concentration (x = 0.0−0.5) of a Secondary Metal (Ti, Zr, and Hf) Added to a WB_4 Alloy, Showing Regions of Solid Solution and Biphasic Mixture[a]

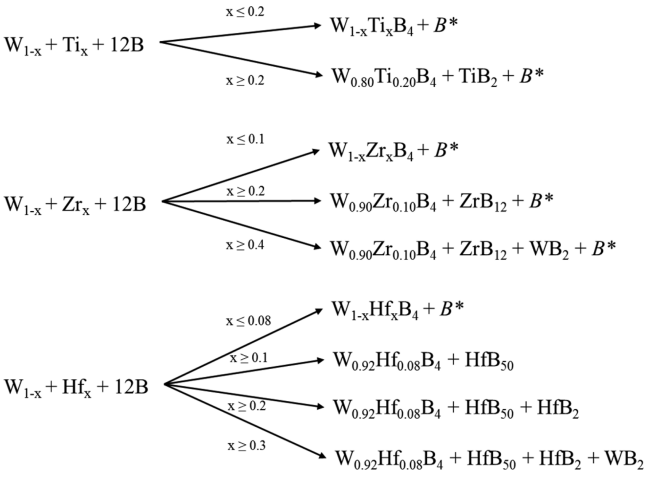

[a] B^* is β-rhombohedral boron.

doping phase of hafnium (H_v ~ 40 GPa at 0.49 N),[16] which is significantly harder than pure β-rhombohedral boron (H_v ~ 34.2 GPa at 0.49 N),[17,18] can provide an additional extrinsic route to hardening the corresponding alloy of WB_4, since tungsten tetraboride requires excess boron in its synthesis in order to avoid the formation of a lower boride (WB_2).

In order to confirm the composition and purity of each sample, EDS was utilized. Additionally, PXRD was used to verify the composition and phase purity. Figure 2a−c shows the PXRD patterns respectively for the alloys $W_{1-x}Ti_xB_4$, $W_{1-x}Zr_xB_4$, and $W_{1-x}Hf_xB_4$. Due to the stoichiometry used for the preparation of the samples, all of them contain some excess crystalline boron, which cannot be observed with ordinary PXRD but are still present in the final ingot. To characterize the excess boron and other secondary phases, EDS analysis was performed on polished samples of $W_{1-x}Ti_xB_4$, $W_{1-x}Zr_xB_4$ and $W_{1-x}Hf_xB_4$, the results of which will be discussed in greater detail later in the paper.

PXRD patterns of the alloys of WB_4 and Ti ($W_{1-x}Ti_xB_4$) are shown in Figure 2a. These patterns indicate that Ti is soluble in WB_4 at or below 20 at. %; at higher concentrations, a secondary phase, TiB_2 (JCPDS 01-075-0967) appears with its corresponding peaks. Note that peaks corresponding to WB_2 (JCPDS 01-073-1244) were not observed in any $W_{1-x}Ti_xB_4$ samples.

PXRD patterns of the alloys of WB_4 and Zr ($W_{1-x}Zr_xB_4$) are shown in Figure 2b. These patterns indicate that Zr is soluble in WB_4 at or below 10 at. %; at a concentration 20 at. % a Zr secondary phase, ZrB_{12} (JCPDS 03-065-7806) appears with its corresponding peaks. Diffraction peaks corresponding to WB_2 (JCPDS 01-073-1244) were observed at 40 at. % Zr for $W_{1-x}Zr_xB_4$ samples.

Powder XRD patterns of the alloys of WB_4 and Hf ($W_{1-x}Hf_xB_4$) are shown in Figure 2c. These patterns indicate that Hf is soluble in WB_4 at or below 8 at. %. At 10 at. % Hf, a secondary phase, HfB_{50} (β-rhombohedral boron doping phase of hafnium, JCPDS 01-086-2400) was observed. At 30 at. % Hf, HfB_2 (JCPDS 01−089−3651) appeared. Diffraction peaks corresponding to WB_2 (JCPDS 01-073-1244) were observed at 30 at. % Hf for $W_{1-x}Hf_xB_4$ samples. The formation of ZrB_{12} and HfB_{50} is thermodynamically favorable, since they are the highest borides for Zr and Hf, respectively, given the stoichiometry used for the preparation of WB_4.[2]

After confirming the composition and purity of the samples using PXRD and EDS, Vickers microindentation hardness measurements were performed on each of the samples under applied loads ranging from 0.49 to 4.9 N. The results of the hardness measurements are shown in Figure 3a−c. For the $W_xTi_{1-x}B_4$ alloy with 8 at. % Ti under a load of 0.49 N, the hardness increased to 50.9 ± 2.2 GPa from 43.3 ± 2.1 GPa[7] for pure WB_4 (corresponding to 0 at. % Ti on the graph). Upon increasing the concentration of Ti, the hardness decreased to 36.3 ± 1.7 GPa at 50 at. % Ti which can be attributed to the formation of TiB_2 as a secondary phase, since the solubility limit for Ti in WB_4 has been exceeded. Similar observations are seen in the measurements carried out under other loads (0.98, 1.94, 2.94, and 4.9 N).

For the $W_{1-x}Zr_xB_4$ alloy with 8 at. % Zr under a load of 0.49 N, the hardness dramatically increased to 55.9 ± 2.7 GPa, followed by a decrease to 45.1 ± 2.6 GPa at 10 at. % Zr. Upon increasing the concentration of Zr, the hardness increased slightly to 46.9 ± 2.3 GPa at 20 at. % Zr, followed by a decrease to 42.6 ± 2.2 GPa at 30 at. % Zr and then increased to 45.6 ± 2.3 GPa at 50 at. % Zr, which can be attributed to the formation of a metal dodecaboride, ZrB_{12} (hardness of ~40 GPa at 0.49 N of force),[19] secondary phase and its competition with WB_4 at higher concentrations of zirconium.

For the $W_{1-x}Hf_xB_4$ alloy with 4−6 at. % Hf under a load of 0.49 N, the hardness increased to 51.3 ± 2.9 GPa and 51.6 ± 2.8 GPa, respectively. The hardness then decreased to 42.2 ± 2.7 GPa at 10 at. % Hf and gradually increased to 45.4 ± 2.2 GPa at 50 at. % Hf, which can be attributed to exceeding the solubility limit of Hf in WB_4 and the formation of the β-rhombohedral boron doping phase of hafnium, HfB_{50}, thus hardening the excess boron. HfB_{50} has a hardness of ~40 GPa at 0.49 N compared to 34.2 GPa at 0.49 N for a sample of crystalline β-rhombohedral boron.[16−18]

The structure of WB_4 has been investigated over many years.[8,11] As established by G. Hägg, in order for higher metal borides (MB_4, MB_6, MB_{12}) to adopt a cubic or hexagonal structure, the ratio of the radius of a boron atom to the radius of a metal atom (Hägg's ratio) should not be above 0.59.[20] The Hägg's ratio for tungsten is R_B/R_W = 0.63 > 0.59, therefore, WB_4 cannot adopt a simple cubic or hexagonal lattice.[3,20] Most recently Lech et al. demonstrated that the crystal structure of WB_4 not only contains partially filled tungsten sites (one-third of W atoms are systematically absent) but also boron trimer sites.[6] Therefore, this unique defect structure of WB_4 could be one of the causes of the hardening for the alloys of WB_4 with Ti, Zr, and Hf (Figure 3a−c).[7] Since Ti, Zr, and Hf are group IV elements, they have two less valence electrons than tungsten. With B occupying the systematic vacant sites of tungsten, the metal atoms can expand the number of boron vacancies.[7]

For the alloy of WB_4 with Ti ($W_{1-x}Ti_xB_4$) at 8 at. % Ti, the valence electron difference in combination with the similar yet slightly greater size of the Ti atom (1.40 Å, compared to 1.35 Å for W)[12] can explain the observed hardness increase. Titanium atoms occupy the positions devoid of tungsten atoms, and the increase in observed hardness is therefore most likely due to solid-solution hardening. TiB_2 is considered the highest boride of Ti, however, titanium can go into a boron matrix and form the β-rhombohedral boron doping phase of titanium (TiB_{50}).[21] Due to the relatively smaller X-ray cross section of titanium (compared to tungsten), this phase does not appear in XRD;

DOI: 10.1021/jacs.6b02676
J. Am. Chem. Soc. 2016, 138, 5714−5721

Figure 2. PXRD patterns of alloys of WB_4 with 2−50 at. % (a) Ti, (b) Zr, and (c) Hf added on a metals basis. The top spectrum in each set is pure WB_4 (JCPDS 00-019-1373). The solubility limit is <20 at. % for Ti, 10 at. % for Zr, and below 8 at. % for Hf. Above 20 at. % Ti, TiB_2 (JCPDS 01-075-0967), above 20 at. % Zr, ZrB_{12} (JCPDS 03-065-7806) and above 10 and 20 at. % Hf, HfB_{50} (β-rhombohedral boron doping phase of hafnium), and HfB_2 (JCPDS 01-086-2400 and 01-089-3651) appear, respectively, as secondary phases. In addition, peaks corresponding to WB_2 (JCPDS 01-073-1244) are observed at 40 at. % Zr and 30 at. % Hf. Full spectra are available in Figure S2.

however, it can be seen using EDS (Figure 4). This can explain the smooth decrease in the hardness at Ti concentrations >10 at. %. As the concentration of Ti increases, it starts to form a TiB_2 secondary phase. While TiB_2 is the hardest AlB_2-type

DOI: 10.1021/jacs.6b02676
J. Am. Chem. Soc. 2016, 138, 5714−5721

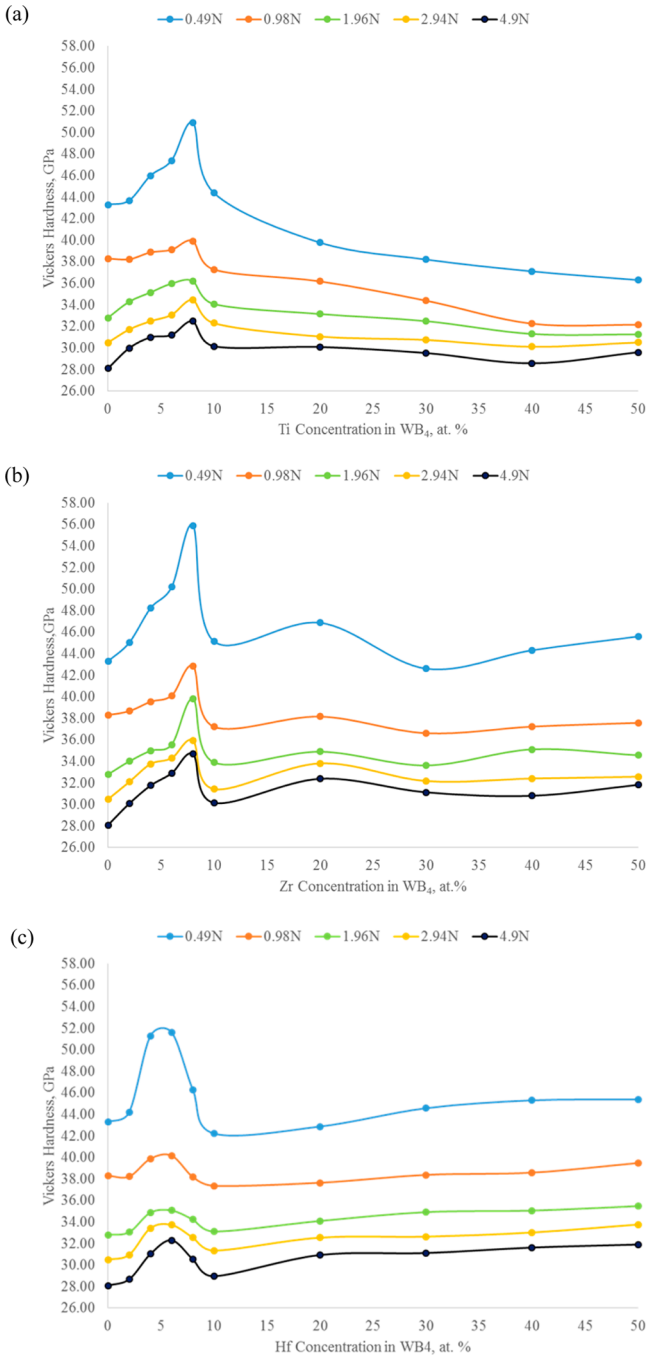

Figure 3. Vickers microindentation hardness of tungsten tetraboride alloys with (a) Ti, (b) Zr, and (c) Hf under 0.49 N (low) to 4.9 N (high) loads. The metal concentrations (x) in $W_{1-x}M_xB_4$ were changed by adding 2−50 at. % Ti, Zr, and Hf on a metals basis.

diboride (hardness of 35 GPa at 0.49 N of force),[22] it is still softer than pure WB_4. This combined with the formation of a β-rhombohedral boron doping phase of titanium, TiB_{50} (hardness of 36.4 GPa at a load of 0.49 N)[18] provides no extrinsic hardening for the $W_{1-x}Ti_xB_4$ alloy and therefore decreases the overall hardness. In addition, it should be noted that the TiB_2 phase is located in the tungsten-rich areas of WB_4, and given the high melting temperature of this phase (3225 °C, compared to 2020 °C for WB_4),[21,23] we can conclude that TiB_2 precipitates out first from the melt and provides a template pattern for the further precipitation of the WB_4 phase (Figure 4); this is known as precipitation hardening.

For the alloy of WB_4 with Zr ($W_{1-x}Zr_xB_4$) at 8 at. % Zr, the valence electron difference and the metal size mismatch (Zr = 1.55 Å, W = 1.35 Å)[12] in combination with the drastic change in grain morphology (Figure 5) can provide a partial explanation for the sharp peak observed in hardness (Figure 3b). Similar to titanium, zirconium atoms can occupy the positions devoid of tungsten atoms and thus increase the hardness due to solid-solution hardening. In contrast to titanium, zirconium's highest boride phase is a metal dodecaboride, ZrB_{12}.[21] Moreover, while Zr also possesses a β-rhombohedral boron doping phase (ZrB_{50}), this does not readily form due to the availability of the higher boride, ZrB_{12} (Figure 6).

Comparing the phase diagrams for the W-boron and Zr-boron systems, there is a similarity to the way both WB_4 and ZrB_{12} form.[23,24] Previous reports indicated that the formation of metal dodecaborides (MB_{12}) is very much dependent on the size of the metal atom in order to accommodate a cuboctahedron unit of boron atoms. Zirconium (1.55 Å)[12] and yttrium (1.80 Å)[12] are the smallest and largest metal atoms, respectively, capable of forming dodecaboride structures.[14,15] While tungsten (1.35 Å)[12] is too small to accommodate a cuboctahedron boron unit and form a dodecaboride, it can be proposed that that $W_{1-x}Zr_xB_4$ alloy can form a metastable dodecaboride that decomposes into the hexagonal WB_4 structure at low concentrations of Zr. The optimal doping amount appears to be 8 at. % Zr in the $W_{1-x}Zr_xB_4$ alloy as seen by the drastic change in morphology (Figure 5).[8,15]

Indeed, the morphology of the 8 at% Zr composition suggests that at high temperatures, the metastable dodecaboride is stabilized. When the arcing is terminated, the sample rapidly cools on the hearth, and the metastable dodecaboride decomposes into two immiscible species: WB_4 and the β-rhombohedral boron doping phase of zirconium (ZrB_{50}); this is known as spinoidal decomposition.[25] Fortuitously, this results in nanostructured grains (Figure 5) and grain hardening. The high density of grain boundaries prevents dislocation propagation and increases the overall hardness of the composite. As such, $W_{0.92}Zr_{0.08}B_4$ (55.9 ± 2.7 GPa at 0.49 N) is 28% harder than its parent WB_4 (43.3 ± 2.1 GPa at 0.49 N). Similar changes in grain morphology and as a result increases in hardness can be expected for other transition metals capable of forming dodecaboride species: scandium and yttrium. Most promisingly, this suggests that decomposition of metastable phases can lead to new routes toward the nanostructuring of superhard grains.

Hardness changes at concentrations of zirconium >10 at. % may be attributed to the following reasons: below 20 at. % zirconium, the ZrB_{12} secondary phase appears, which hardens the material through a dispersion hardening mechanism. At higher concentrations of zirconium, both ZrB_{12} and WB_4 phases form, which are the highest borides of zirconium and tungsten, respectively, and they compete with one another. The hardness of $W_{1-x}Zr_xB_4$ gently increases as x approaches 50 at. % Zr and more ZrB_{12} is formed.

For the alloy of WB_4 with Hf ($W_{1-x}Hf_xB_4$) at 4−6 at. % Hf, the valence electron difference and the metal size mismatch (Hf = 1.55 Å, W = 1.35 Å)[12] may provide an explanation for the broad hardness peak with hardness values increasing to 51.3 ± 2.9 and 51.6 ± 2.8 GPa at 0.49 N, respectively, compared to 43.3 ± 2.1 GPa at 0.49 N for pure WB_4 (Figure 3c). Similar to

DOI: 10.1021/jacs.6b02676
J. Am. Chem. Soc. 2016, 138, 5714−5721

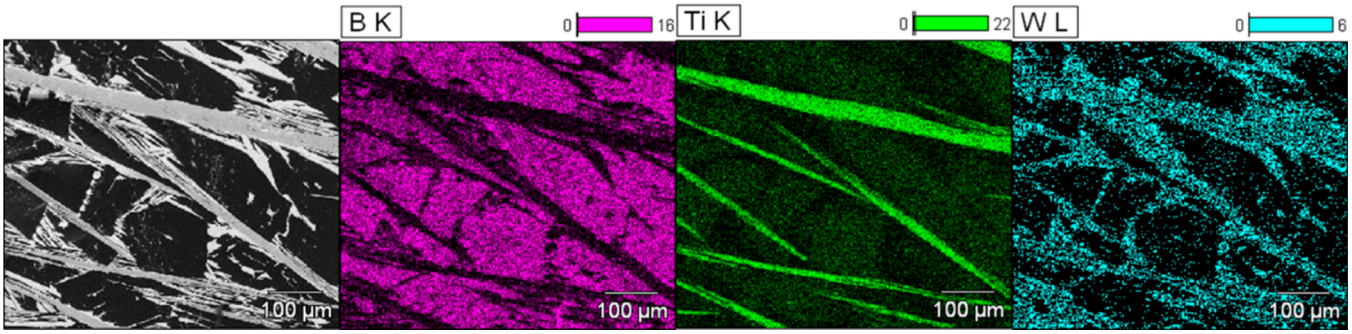

Figure 4. Elemental maps for boron (K line), titanium (K line), and tungsten (L line) for the $W_{0.50}Ti_{0.50}B_4$ alloy showing the presence of titanium in TiB_{50} (β-rhombohedral boron doping phase of titanium) corresponding to boron-rich areas and TiB_2 in tungsten-rich areas.

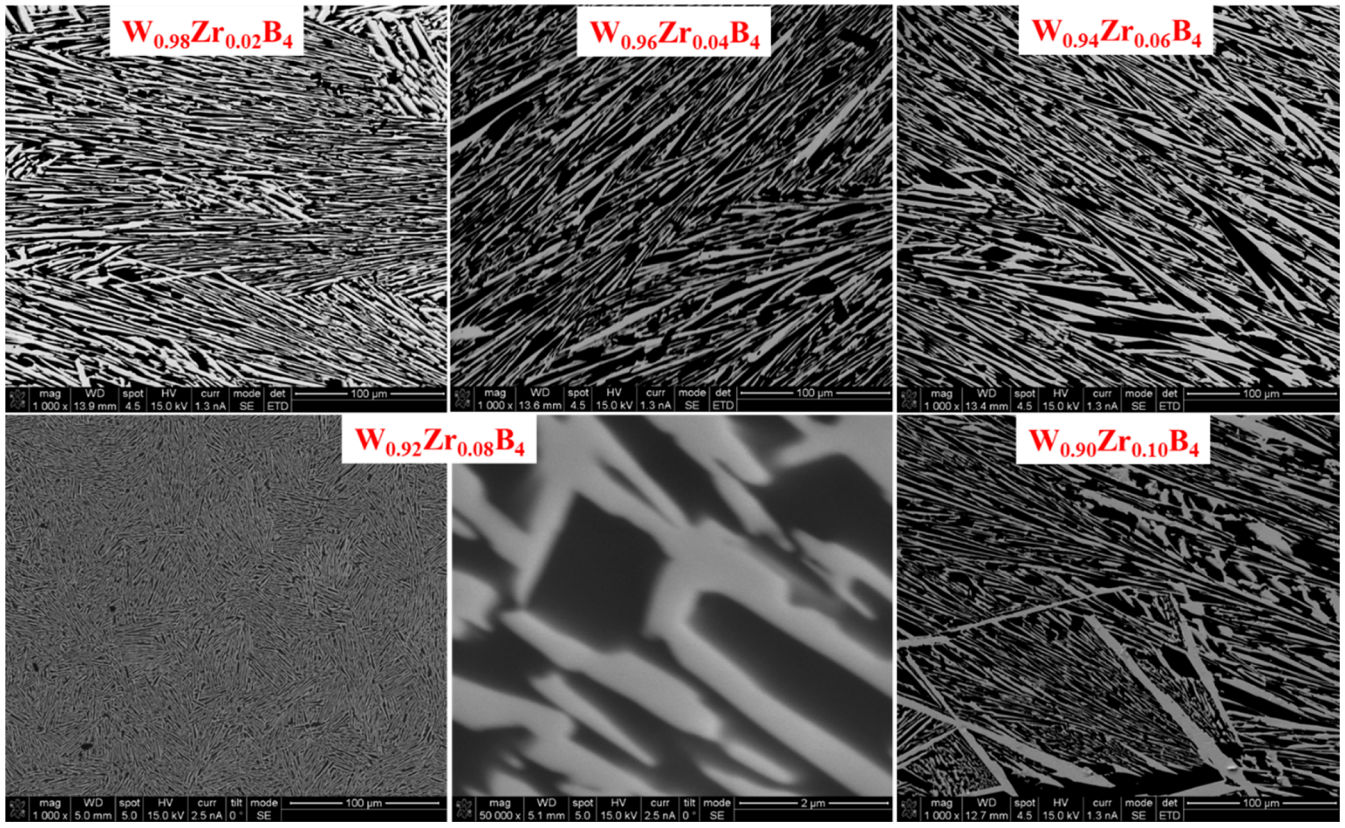

Figure 5. SEM images of the alloys of WB_4 with 2−10 at. % Zr taken at 1000× magnification and 50,000× for the hardest composition, $W_{0.92}Zr_{0.08}B_4$, showing changes in morphology. The drastic change of surface morphology at 8 at. % Zr can be attributed to a decomposition from a metastable W−Zr dodecaboride phase.

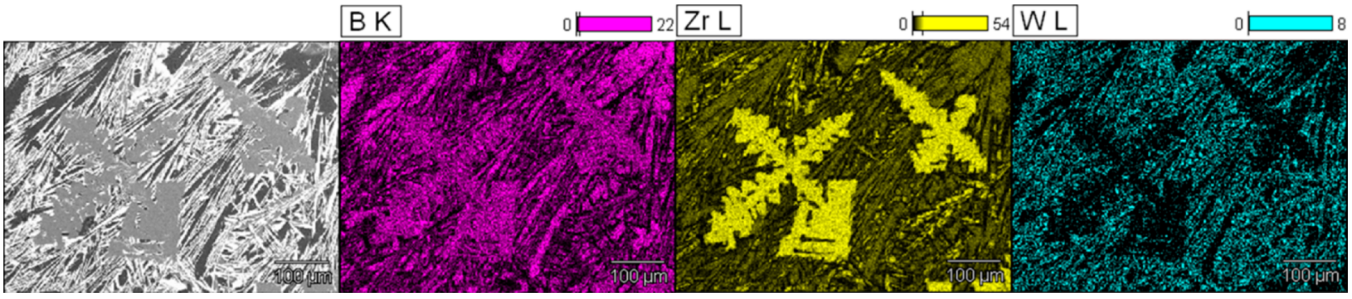

Figure 6. Elemental maps for boron (K line), zirconium (L line), and tungsten (L line) for the $W_{0.50}Zr_{0.50}B_4$ alloy showing the presence of zirconium in ZrB_{12} and no formation of ZrB_{50} (the β-rhombohedral boron doping phase of zirconium).

titanium and zirconium, hafnium atoms can occupy the positions of the missing tungsten atoms, and the increase in hardness is therefore most likely due to solid-solution hardening. Similar to titanium, hafnium's highest boride

DOI: 10.1021/jacs.6b02676
J. Am. Chem. Soc. 2016, 138, 5714−5721

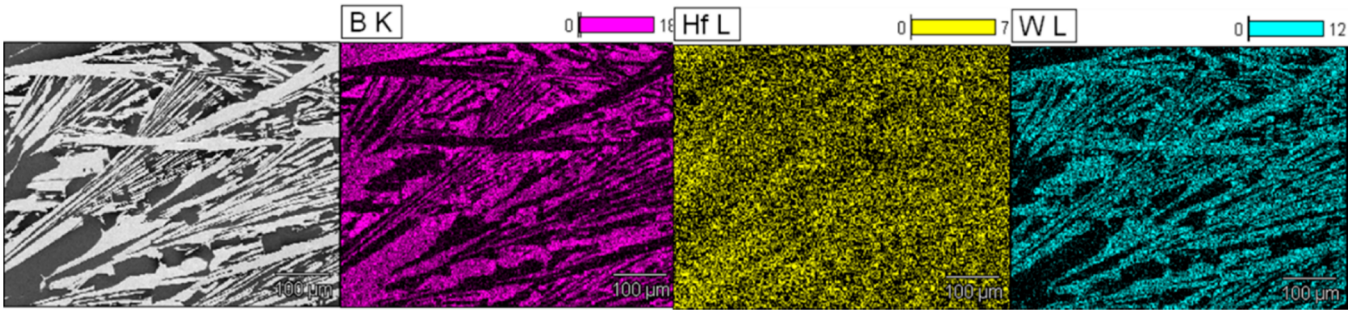

Figure 7. Elemental maps for boron (K line), hafnium (L line), and tungsten (L line) for the $W_{0.90}Hf_{0.10}B_4$ alloy showing the presence of hafnium in WB_4 as well as in the boron-rich phase (known as the β-rhombohedral boron doping phase of hafnium −HfB_{50}).

phase is the diboride HfB_2; however, it also forms the β-rhombohedral boron doping phase of hafnium, HfB_{50}.[16] In contrast to TiB_{50}, hafnium has a large enough X-ray cross-section for the HfB_{50} phase to appear in the PXRD spectrum (Figure 2c). Due to the lanthanide contraction, for most purposes zirconium and hafnium have essentially the same atomic radius (1.55 Å).[12] Thus, in contrast to zirconium, hafnium does not form a dodecaboride phase under ambient pressure; however, it can be synthesized with the application of 6.5 GPa of pressure.[14] This is due to the fact that in a 12-coordinate environment, zirconium and hafnium have different metallic radii: 1.603 and 1.580 Å, respectively.[14]

The HfB_{50} phase appears as a secondary phase at 10 at. % Hf (Figure 2c). Figure 7 shows the elemental maps of a sample of an alloy of WB_4 with 10 at. % Hf ($W_{0.90}Hf_{0.10}B_4$). Note that hafnium is present not only in the tungsten-rich areas (showing the presence of Hf in the WB_4 lattice) but also in boron-rich areas (forming HfB_{50}). As the concentration of hafnium increases, it extrinsically hardens WB_4 by hardening the excess crystalline boron (H_v = 34.2 GPa at 0.49 N)[17,18] (Figure 3c) through the formation of a β-rhombohedral boron doping phase of hafnium, HfB_{50}, (H_v ~ 40 GPa at 0.49 N).[16]

Table 1 compares the values of hardness for the hardest compositions of alloys of WB_4 with Ti, Zr, and Hf with those of pure WB_4 and the hardest WB_4 alloy reported, $W_{0.93}Ta_{0.02}Cr_{0.05}B_4$.[7] Both $W_{0.93}Ta_{0.02}Cr_{0.05}B_4$ and $W_{0.92}Zr_{0.08}B_4$ have similar total secondary metal content, 7−8 at. %, and while $W_{0.92}Zr_{0.08}B_4$ is slightly softer than $W_{0.93}Ta_{0.02}Cr_{0.05}B_4$ at low load (0.49 N), it exhibits increased hardness values at higher loads, indicating a smaller influence of the indentation size effect due to the extremely fine surface morphology of this sample (Figure 6).

Table 1. Vickers Microindentation Hardness Data for the Hardest Alloys of WB_4 with Ti, Zr, and Hf[a]

	applied load (N)				
compd/alloy	0.49	0.98	1.96	2.94	4.9
WB_4	43.4	38.3	32.8	30.5	28.1
$W_{0.93}Ta_{0.02}Cr_{0.05}B_4$	57.3	44.1	38.2	34.8	31.7
$W_{0.92}Ti_{0.08}B_4$	50.9	39.9	36.2	34.5	32.5
$W_{0.92}Zr_{0.08}B_4$	55.9	42.9	39.8	35.9	34.7
$W_{0.94}Hf_{0.06}B_4$	51.6	40.2	35.1	33.7	32.3

[a]Hardness data for pure WB_4 and $W_{0.93}Ta_{0.02}Cr_{0.05}B_4$ alloy are presented for comparison.[7]

Oxidation resistance is an important parameter for materials used for cutting and machining tools. As such, in order to test the thermal stability of the samples of alloys of Ti, Zr, and Hf with WB_4, TGA in air was performed on the samples with the compositions corresponding to the hardest alloys. Figure S3 summarizes the results.

The TGA data indicate that alloys of Ti, Zr and Hf with WB_4 have enhanced oxidation properties in comparison to pure WB_4 and the hardest tantalum−chromium alloys of WB_4 ($W_{0.93}Ta_{0.02}Cr_{0.05}B_4$). $W_{0.92}Ti_{0.08}B_4$, $W_{0.92}Zr_{0.08}B_4$, and $W_{0.94}Hf_{0.06}B_4$ are stable up to ~460 °C, ~ 510 °C, and ~490 °C, respectively, compared to ~400 °C for pure WB_4 and ~420 °C for $W_{0.93}Ta_{0.02}Cr_{0.05}B_4$. The products of oxidation are WO_3 and TiO_2 for $W_{0.92}Ti_{0.08}B_4$, WO_3 and ZrO_2 for $W_{0.92}Zr_{0.08}B_4$, and WO_3 and HfO_2 for $W_{0.94}Hf_{0.06}B_4$ samples, as determined by PXRD analysis. Thus, an increase of about 100 °C in stability is observed for the hardest zirconium alloy of WB_4, which has a comparable hardness to that of $W_{0.93}Ta_{0.02}Cr_{0.05}B_4$.

CONCLUSIONS

Alloys of WB_4 with the group 4 transition metals (Ti, Zr and Hf) were synthesized, and their hardness and thermal stability characterized. These alloys are interesting due to the higher boride phases they can form: metal dodecaboride and β-rhombohedral boron doping phases. Doping with 8% Ti ($W_{0.92}Ti_{0.08}B_4$), 8% Zr ($W_{0.92}Zr_{0.08}B_4$), and 6% Hf ($W_{0.94}Hf_{0.06}B_4$) showed the highest values of hardness (at 0.49 N applied load) for their respective alloys: 50.9 ± 2.2, 55.9 ± 2.7, and 51.6 ± 2.8 GPa, compared to 43.3 ± 2.1 GPa for pure WB_4. Electronic effects from valence electron mismatch (4 electrons for group 4 metals and 6 electrons for tungsten from group 6) or atomic size mismatch (W = 1.35 Å, Ti = 1.40 Å, Zr = 1.55 Å, Hf = 1.55 Å)[12] are the likely cause of the increase in hardness at low concentrations of Ti, Zr and Hf. In addition, the alloys of WB_4 with zirconium and hafnium showed extrinsic hardening at higher concentrations of these transition metals. Alloys of WB_4 with zirconium showed drastic changes in the surface morphology of the corresponding samples at <10 at. % Zr, likely due to the formation of a metastable Zr−W dodecaboride phase. This can be attributed to the formation of the hard metal dodecaboride phase (ZrB_{12}) for zirconium and hardening of the excess boron, through the formation of β-rhombohedral boron doping phase (HfB_{50}) for hafnium. In addition, the alloys of titanium, zirconium, and hafnium with WB_4 showed increased oxidation resistance up to ~460 °C, ~ 510 °C, and ~490 °C, respectively, compared to ~400 °C for pure WB_4. By adding to WB_4 other metals with larger atomic radii than tungsten that possess different higher boride phases, such as YB_{66}[26] for yttrium and ScB_{19}[27] for scandium, their effects on the resulting alloys can be studied, and other possible hardening mechanisms explored.

DOI: 10.1021/jacs.6b02676
J. Am. Chem. Soc. 2016, 138, 5714−5721

■ ASSOCIATED CONTENT

Supporting Information

The Supporting Information is available free of charge on the ACS Publications website at DOI: 10.1021/jacs.6b02676.

Crystal structure of β-rhombohedral boron and β-rhombohedral boron doping phase of hafnium. XRD data obtained for ternary alloys of WB_4 with Ti, Zr and Hf. TGA data for the hardest alloys of WB_4 with Ti, Zr and Hf (PDF)

■ AUTHOR INFORMATION

Corresponding Author

*kaner@chem.ucla.edu

Notes

The authors declare no competing financial interest.

■ ACKNOWLEDGMENTS

We thank the National Science Foundation Division of Materials Research, Grant DMR-1506860 (R.B.K.), Virginia Commonwealth University Startup Grant 137422 (R.M.), and the National Science Foundation DGE-0654431 Fellowship program (M.T.Y.) for financial support and Professor Benjamin M. Wu of the UCLA Department of Bioengineering for the use of the microindentation system in his laboratory.

■ REFERENCES

(1) Yeung, M. T.; Mohammadi, R.; Kaner, R. B. *Annu. Rev. Mater. Res.* **2015**, *46*, 2.1−2.21.

(2) Samsonov, G. V. *Borides [in Russian]*; Atomizdat: Moscow, 1975.

(3) Samsonov, G. V., Markovskii, L. Y. *Boron, Its Compounds and Alloys [in Russian]*; House of the Academy of the Sciences Ukrainian SSR: Kiev, 1960.

(4) Mohammadi, R.; Kaner, R. B. Superhard Materials. In *Encyclopedia of Inorganic and Bioinorganic Chemistry*; Scott, R.A. Ed., John Wiley and Sons, Inc.: Hoboken, NJ, 2012; pp 1−19.

(5) Kaner, R. B.; Gilman, J. J.; Tolbert, S. H. *Science* **2005**, *308*, 1268−1269.

(6) Lech, A. T.; Turner, C. L.; Mohammadi, R.; Tolbert, S. H.; Kaner, R. B. *Proc. Natl. Acad. Sci. U. S. A.* **2015**, *112*, 3223−3228.

(7) Mohammadi, R.; Xie, M.; Lech, A. T.; Turner, C. L.; Kavner, A.; Tolbert, S. H.; Kaner, R. B. *J. Am. Chem. Soc.* **2012**, *134*, 20660−20668.

(8) Mohammadi, R.; Lech, A. T.; Xie, M.; Weaver, B. E.; Yeung, M. T.; Tolbert, S. H.; Kaner, R. B. *Proc. Natl. Acad. Sci. U. S. A.* **2011**, *108*, 10958−10962.

(9) Mohammadi, R.; Turner, C. L.; Xie, M.; Yeung, M. T.; Lech, A. T.; Tolbert, S. H.; Kaner, R. B. *Chem. Mater.* **2016**, *28*, 632−637.

(10) Bodrova, L. G.; Koval'chenko, M. S.; Serebryakova, T. I. *Sov. Powder Metall. Met. Ceram* **1974**, *13*, 1−3.

(11) Romans, P. A.; Krug, M. P. *Acta Crystallogr.* **1966**, *20*, 313−315.

(12) Slater, J. C. *J. Chem. Phys.* **1964**, *41*, 3199−3204.

(13) Kittel, C. *Introduction to Solid State Physics*, 8th ed.; Johnson, S., Ed.; John Wiley & Sons: Hoboken, NJ, 2005.

(14) Cannon, J. F.; Farnsworth, P. B. *J. Less-Common Met.* **1983**, *92*, 359−368.

(15) La Placa, S.; Binder, I.; Post, B. *J. Inorg. Nucl. Chem.* **1961**, *18*, 113−117.

(16) Portnoi, K. I.; Romashov, V. M.; Romanovich, I. V.; L, Y. V. *Inorg. Mater.* **1971**, *7*, 1769−1772.

(17) Andersson, S.; Lundström, T. *J. Solid State Chem.* **1970**, *2*, 603−611.

(18) Carlsson, J.-O.; Lundström, T. *J. Less-Common Met.* **1970**, *22*, 317−320.

(19) Kuzenkova, M. A.; Kislyi, P. S. *Powder Metall.* **1965**, *4*, 966−969.

(20) Hägg, G. *Z. Phys. Chem.* **1931**, *B12*, 33.

(21) Murray, J. L.; Liao, P. K.; S, K. E. *Bin. Alloy Phase Diagrams* **1990**, *1*, 544−548.

(22) Basu, B.; Raju, G. B.; Suri, A. K. *Int. Mater. Rev.* **2006**, *51*, 352−374.

(23) Duschanek, H.; Rogl, P. *J. Phase Equilib.* **1995**, *16*, 150−161.

(24) Portnoi, K. I. *Sov. Powder Met. Met. Ceram.* **1970**, *9*, 577−580.

(25) Cahn, J. W. *Acta Metall.* **1961**, *9*, 795−801.

(26) Richards, S. M.; Kaspar, J. S. *Acta Crystallogr., Sect. B: Struct. Crystallogr. Cryst. Chem.* **1969**, *25*, 237−251.

(27) Tanaka, T.; Okada, S.; Gurin, V. *J. Alloys Compd.* **1998**, *267*, 211−214.

DOI: 10.1021/jacs.6b02676
J. Am. Chem. Soc. 2016, 138, 5714−5721